Valence-band structure of epitaxially grown $Fe_3O_4(111)$ films

Y. Q. Cai,* M. Ritter, W. Weiss, and A. M. Bradshaw
Fritz-Haber-Institut der Max-Planck-Gesellschaft, Faradayweg 4-6, 14195 Berlin-Dahlem, Germany
(Received 26 January 1998; revised manuscript received 22 April 1998)

It has recently been shown that well-ordered $Fe_3O_4(111)$ films can be prepared epitaxially on clean Pt(111) surfaces; various techniques have indicated that these multilayer films are chemically identical to bulk single crystals. We have studied the electronic structure of such an ordered $Fe_3O_4(111)$ film using angle-resolved photoemission in conjunction with synchrotron radiation. The valence-band structure along the ΓL symmetry line and the resonant emission enhancement across the Fe $3p \rightarrow 3d$ excitation threshold have been examined in detail both above (at 300 K) and below (at 90 K) the Verwey transition temperature ($\sim$120K) for magnetite. The observed band dispersion agrees reasonably well with band-structure calculations for the high-temperature phase, particularly near the Fermi level, suggesting that Fe_3O_4 should be treated with band theory. Subtle differences in the valence-band structure are observed between the two temperatures, which may be attributed to a structural change and/or a charge ordering associated with the Verwey transition. The resonant behavior shows, however, no temperature dependence, indicating that resonant photoemission in Fe_3O_4 remains a localized process and is not influenced by the Verwey transition. [S0163-1829(98)01231-4]

I. INTRODUCTION

Single-crystal metal oxide thin films grown epitaxially on conducting substrates have recently attracted increased attention in surface science. The cleanliness, stoichiometry, and crystalline order of the surface of these thin oxide films can be well controlled, and yet structurally and chemically they are found to be identical with their bulk counterparts.[1–5] Furthermore, for insulating oxides, the electrostatic charging problem associated with the use of ultrahigh-vacuum (UHV) based spectroscopic techniques that involve the emission and/or scattering of charged particles can be eliminated. These thin oxide films, therefore, provide opportunities for spectroscopic studies of the electronic structure of metal oxides, which is a prerequisite for understanding the physical principles governing their interesting electrical and magnetic properties.[6] Moreover, they can be used for studying the surface chemistry of metal oxides, which is in turn important for addressing the issues in metal-oxide-based catalysis.[7] The present paper reports a photoemission study on such an ordered, thin iron oxide film, i.e., $Fe_3O_4(111)$, grown epitaxially on a clean Pt(111) substrate.[1–3]

Fe_3O_4 (magnetite) is a ferrimagnet with the cubic inverse spinel structure.[6] At room temperature the lattice has fcc symmetry and consists in a purely ionic model of a close-packed face-centered cube of large O^{2-} anions with the smaller cations, Fe^{2+} and Fe^{3+}, located in the interstitial sites of the anion lattice. Two kinds of cation sites exist in the crystal: One site designated A is tetrahedrally coordinated to oxygen and is occupied only by Fe^{3+} ions. The other site designated B is octahedrally coordinated to oxygen and is occupied by equal numbers of Fe^{2+} and Fe^{3+} ions.

The valence electronic structure and the Verwey transition of magnetite have been intensively studied in the past both theoretically [8–13] and experimentally.[3,8,14–23] The Verwey transition is characterized by a sharp decrease in the conductivity by two orders of magnitude at a temperature of $T_v \sim 120$ K, accompanied by a crystallographic structural change from cubic to monoclinic.[24,25] From a localized-electron point of view, the high electrical conductivity of magnetite at room temperature is attributed to electron hopping between the Fe^{2+} and the Fe^{3+} ions occupying the B site. The Verwey transition[24] freezes these electrons and causes an ordering of the extra electron (compared to Fe^{3+}) at the Fe^{2+} B site at temperatures below T_v, although the precise ordering is still unclear.[10,13] The same phenomenon, however, can also be considered from an itinerant-electron point of view: The high conductivity is a natural consequence of the half-filled $3d$ band of iron atoms located at the B site, and the Verwey transition results from a band splitting due to the increasing importance of electron-electron correlation and/or electron-phonon interactions at low temperatures.[6]

The interpretation of the valence-band photoemission spectra from Fe_3O_4 and the other iron oxides has long been a matter of debate. Early studies were mostly interpreted on the basis of the ligand-field theory,[26] in which the localized $3d$ cation levels, split further by the oxygen ligand field, were found responsible for the photoemission features, rather than the bandlike $3d$ density of states.[15,27] Further studies found that it was necessary to include configuration interaction (CI) within the $3d$ multiplet and charge transfer between the $3d$ and the ligand orbitals to improve the agreement with experiment and to account for the satellite features observed in photoemission.[28,29] Resonant photoemission across the Fe $3p \rightarrow 3d$ excitation threshold was also used to identify the nature of the photoemission features near the Fermi level. It led to the conclusion that the occupied states near the Fermi level are mainly of $3d^n\underline{L}$ ($\underline{L}$ represents a ligand hole) character and that all iron oxide phases (FeO, Fe_3O_4, and α-Fe_2O_3) should be classified as charge-transfer insulators.[19,29,30] In contrast, recent O K-edge x-ray absorption and emission experiments on Fe_3O_4 suggested that the states on both sides of the band gap are of $3d$ origin and Fe_3O_4 should therefore be considered as a Mott-Hubbard

insulator.[20,22] Furthermore, inverse photoemission experiments[21,31,32] probing the states above the Fermi level revealed various degrees of covalency for all the iron oxide phases and found, in the case of Fe_2O_3, that the on-site d-d Coulomb interaction energy (U) was overestimated by the CI theory.

All these interpretations that were based on the localized-electron point of view did not take into account the anisotropy and translational symmetry of the crystal, and therefore could not explain itinerant properties of the electronic structure such as band dispersion. So far, there has been only one study[18] in which experimental photoemission spectra were interpreted with the help of a band-structure calculation for magnetite.[11] The study was performed on an *in situ* cleaved $Fe_3O_4(100)$ single crystal at room temperature. Finite intensity existed at the Fermi level, which indicated that Fe_3O_4 is a metal rather than an insulator, in agreement with the band-structure calculation. Although energy-band dispersion as predicted by the calculation was not clearly observed, it was concluded that the itinerant-electron description is more appropriate than the localized-electron point of view for describing the electronic structure of Fe_3O_4.[11,18]

This is confirmed by the present study on an $Fe_3O_4(111)$ thin film using angle-resolved photoemission in conjunction with synchrotron radiation. We observe clear dispersion of several distinct features along the ΓL direction in our spectra, which qualitatively agrees with band-structure calculations.[11,12,33] In addition, the change in the electronic structure across the Verwey transition is examined by taking spectra both at 300 and 90 K. Subtle differences have been observed and may be understood on the basis of changes in crystalline structure and/or by the ordering of the cations occupying the B site associated with the transition. The resonant behavior across the Fe $3p \rightarrow 3d$ excitation threshold and its temperature dependence is also examined in detail. These results are discussed in terms of both the itinerant-electron and localized-electron descriptions.

II. EXPERIMENTAL DETAILS

Experiments were carried out in an UHV chamber on two different toroidal grating monochromator beamlines (TGM3 and TGM4) at the Berlin synchrotron radiation source (BESSY). The chamber was equipped with a VG Instruments ADES400 spectrometer for angle-resolved photoemission measurements and a Varian LEED (low-energy electron diffraction) optics for the determination of surface periodicity. The overall energy resolution depends on the settings of the monochromator and of the spectrometer, and was maintained at around 150 meV for all the measurements reported here. The angular resolution was $\pm 1°$. The base pressure after bakeout was 2×10^{-10} mbar.

The Pt(111) crystal was mounted on a manipulator where it could be heated resistively and cooled with liquid nitrogen. The sample temperature was measured with a Chromel-Alumel thermocouple spotwelded to the back of the crystal. The Pt(111) surface was cleaned by repeated cycles of 1-keV Ar^+ ion bombardment and subsequent annealing to $T=1350$ K in 10^{-7}-mbar oxygen atmosphere to remove the carbon contaminants on the surface. A final flash to 1350 K resulted in a clean and well-ordered surface as judged by a sharp hexagonal 1×1 LEED pattern and photoemission spectra that show no signs of contamination in the valence-band region [Fig. 1(a)].

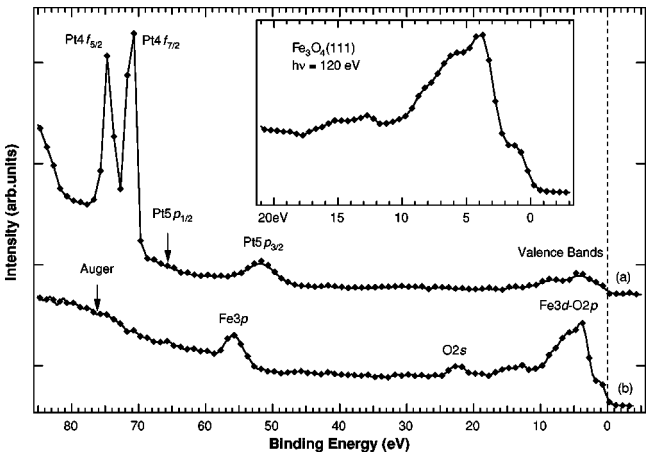

FIG. 1. Ultraviolet photoemission spectroscopy spectra giving an overview for (a) the clean Pt(111) surface ($h\nu=150$ eV), and (b) the Fe_3O_4 film ($h\nu=120$ eV). Binding energy is relative to the Fermi edge of the clean Pt(111) surface. The inset shows the Fe_3O_4 valence features on an expanded scale.

The Fe_3O_4 film was prepared following the method described in detail elsewhere.[1,34] In summary, it started with the vapor deposition of submonolayer of iron onto the clean Pt(111) surface at room temperature, followed by heating for 2–3 min in 1×10^{-6} mbar oxygen at temperatures around 1000 K. This produced a well-ordered oxide layer with the stoichiometry and structure of a FeO(111) bilayer.[1,34] The latter can be identified by its characteristic LEED pattern, which consists of the main FeO and Pt diffraction spots surrounded by a rosette of six satellite features with uniform intensity. A detailed scanning tunneling microscopy investigation has revealed that the iron oxide grows in a Stranski-Krastanov mode after repeated iron deposition and oxidation cycles.[34] It grows layer by layer in the FeO structure up to 2 ML thickness; subsequently, $Fe_3O_4(111)$ islands begin to form and finally coalesce to give a thick film. By this time the satellite spots have disappeared and a new 2×2 LEED pattern characteristic of the $Fe_3O_4(111)$ surface is observed. X-ray photoelectron and Auger electron spectroscopy studies[1–3] of this oxide film have revealed the Fe_3O_4 stoichiometry, and a dynamic LEED intensity analysis[1] has shown a strongly relaxed, unreconstructed $Fe_3O_4(111)$ surface. The final thickness of the film was estimated to be at least 60 Å; no emission from the Pt $4f$ core level and the Pt valence bands can be seen [for example, in Fig. 1(b) (Ref. 35)]. The Pt substrate thus has only a negligible influence on the photoemission spectra discussed in the next section.

Angle-resolved photoemission spectra were recorded at normal emission both at 90 and 300 K (room temperature). Polarized light was incident on the surface at an angle of 45° with the electric vector **E** in the plane spanned by the [111] and the $[\bar{1}10]$ axes.

III. RESULTS AND DISCUSSION

A selection of the normal emission spectra [energy distribution curves] taken at room temperature (300 K) is shown

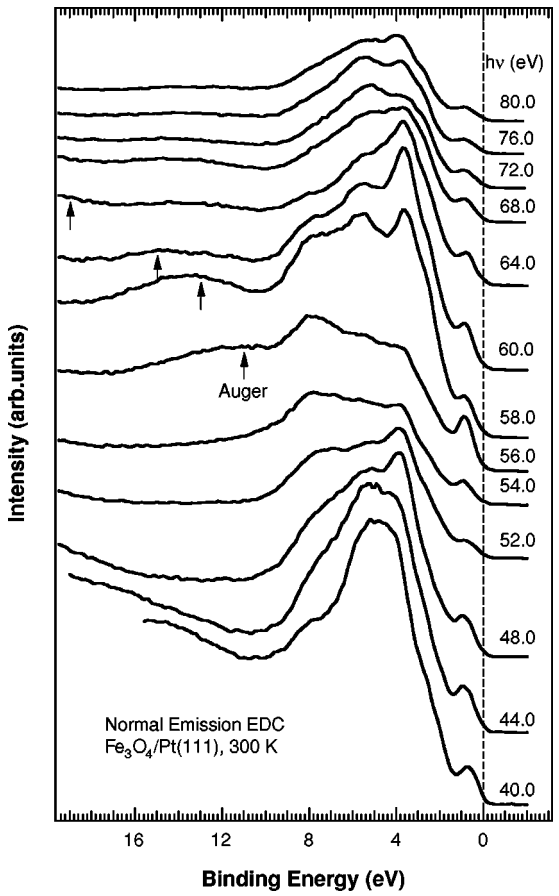

FIG. 2. Normal-emission spectra from the valence bands of Fe_3O_4 taken at room temperature (300 K). The binding energy is measured relative to the Fermi edge of the Pt substrate. Arrows indicate the expected positions for the $M_{2,3}M_{4,5}M_{4,5}$ Auger emission for photon energies above the Fe $3p$ excitation threshold (56 eV).

in Fig. 2; the Fermi level corresponds to that of the platinum substrate. The photon energy was tuned in 1 eV steps over the range 40–80 eV, which includes the Fe $3p \rightarrow 3d$ excitation threshold at 56 eV where strong resonant photoemission is observed. The spectra are normalized to the photon flux recorded by the photoelectric yield of the Au-coated refocusing mirror of the beamlines (not corrected for the quantum efficiency[36]).

There is finite photoemission intensity at the Fermi level in all spectra, which is clearly due to the feature at the lowest binding energy and is compatible with the high conductivity of magnetite seen for bulk single crystals.[18,19] The defect concentration is not known, which may also play a role in contributing to the intensity at the Fermi level through impurity scattering of the photoelectrons in the present case. Within the binding energy range shown, several features are visible. The valence bands derived from the Fe $3d$ and O $2p$ orbitals between 0 and 10 eV binding energy show considerable variation both in intensity and spectral line shape as a function of photon energy. Some peaks disperse (see below) and are better resolved than spectra taken from cleaved single-crystal surfaces in earlier studies.[18,19] A possible reason is that the thin-film surface prepared in the present study is of much higher quality compared to the cleaved surfaces and k smearing caused by surface roughness is less of a problem. A thorough examination of the structure in this region will be reported in Sec. III A. Above the Fe $3p \rightarrow 3d$ excitation threshold at $h\nu = 56$eV, a strong enhancement of the valence bands and of the broad satellite feature centered at 14 eV is observed. This broad satellite feature is also visible at higher photon energies [see Fig. 1(b) and the inset]. The $M_{2,3}M_{4,5}M_{4,5}$ super-Coster-Kronig Auger transitions appear with a constant kinetic energy of 45 eV with respect to the Fermi edge[29] and are indicated by the arrows. These Auger transitions are in general weak and broad, but are much enhanced within the resonant region. The resonant photoemission data will be discussed in Sec. III B.

A. Band dispersion

In order to examine in detail the valence bands of Fe_3O_4 observed in Fig. 2, we will compare our experimental results with first-principles calculations. The first realistic band-structure calculation for Fe_3O_4 in the high-temperature phase was carried out by Yanase and Siratori[11] (YS) in 1984 using the self-consistent augmented plane waves (APW) method. Exchange and correlation energies were considered under the local spin-density approximation (LSDA). Later Zhang and Satpathy [12] (ZS) reported another LSDA calculation using the self-consistent linear muffin-tin orbitals method in the atomic spheres approximation. This calculation agrees in general with that of YS, particularly with respect to the metallic nature of magnetite and the Fe $3d$ origin of the states located up to 1 eV below the Fermi energy. These results were supported by experimental data from spin-polarized photoemission[15] and polarized neutron scattering.[37] More recently, Yanase and Hamada (YH) have performed a full-potential linearized APW calculation within the LSDA for magnetite[33] in order to obtain the precise shape of the Fermi surface and the charge density. The resulting band structure and the partial one-electron density of states are very similar to the earlier calculations of YS and ZS, although the exact location and dispersion of various bands differ somewhat in the three calculations.[11,12,33] The charge density obtained in the latest calculation is found to agree well with results from x-ray diffraction studies[33] and therefore supports the local-density approximation used in the calculation.[38]

A comparison between our normal emission data and the YH band-structure calculation is shown in Figs. 3 and 4 in the form of structure plots for data taken at 300 and 90 K,[39] respectively. Experimental points are peak or shoulder positions in the EDC's determined from the local minima positions in the second derivative of the smoothed curves.[40] A potential shortcoming of this data analysis method is that some finer details may be lost due to the smoothing prior to taking the derivatives, and that in a spectral region where many closely spaced bands may contribute, the resulting points may not necessarily reflect the true situation. We are aware of these problems but, nevertheless, believe that the present analysis yields the dominant information accessible under our energy and angular resolution in the experiment.

The resulting peaks and shoulders are divided further into strong and weak transitions based on the absolute intensity of the minima of the second derivative curves. The calculated transitions (solid lines) represent direct transitions satisfying[41]

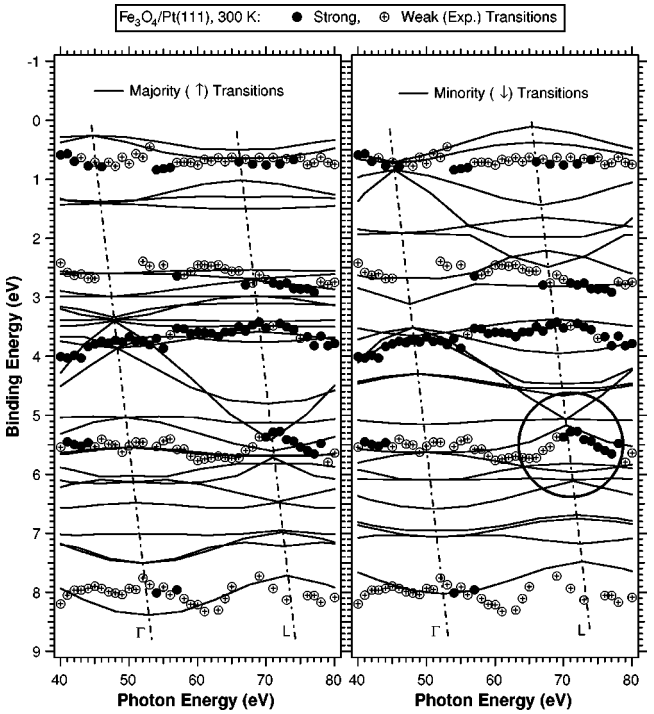

FIG. 3. Structure plot for normal emission data (points) taken at 300 K. Experimental data shown in the left and right panels are the same but theoretical direct transitions (solid lines) are calculated using the band structure of the majority spin (left panel) and of the minority spin (right panel) by YH and free-electron final states. The circled region is for comparison with Fig. 4. See text for details.

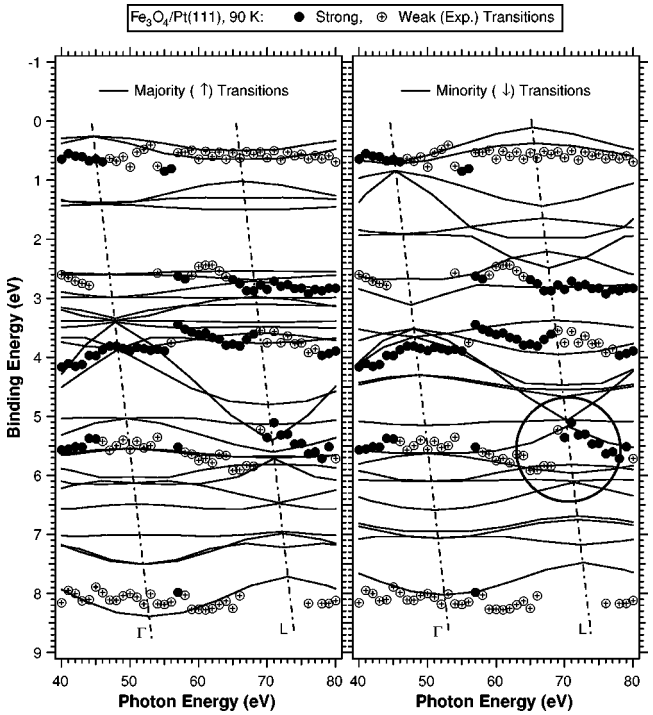

FIG. 4. Same as Fig. 3 but for the normal emission data taken at 90 K.

$$h\nu = E_f(\mathbf{k}^{\parallel},\mathbf{k}^{\perp}) - E_i(\mathbf{k}^{\parallel},\mathbf{k}^{\perp}). \tag{1}$$

The initial state energies E_i are given by the band structure calculated by YH, and the final state energies E_f are free-electron final states of the form

$$E_f(\mathbf{k}^{\parallel},\mathbf{k}^{\perp}) = \frac{\hbar^2}{2m}(\mathbf{k}^{\perp}+\mathbf{k}^{\parallel}+\mathbf{G})^2 - E_0, \tag{2}$$

where $(\mathbf{k}^{\parallel},\mathbf{k}^{\perp})$ is the wave vector of the electron, the parallel component $\mathbf{k}^{\parallel}=0$ for normal emission, and the perpendicular component $0 \leqslant k^{\perp} \leqslant \sqrt{3}\pi/a$ for Γ-L, a being the lattice constant; E_0 is the inner potential with respect to the Fermi level; $\mathbf{G}[=(2\pi/a)(l,m,n)]$ is a bulk reciprocal lattice vector. Only the primary cone with $(l,m,n)=(I,I,I)$, where $I=0,\pm 1,\pm 2,\ldots$, is used here. For clarity and for identifying the spin character of the observed experimental features, calculated transition lines using the initial majority- and minority-spin bands are shown separately in the left and right panels of Figs. 3 and 4, respectively.

As can be seen, data taken at 300 and 90 K are quite similar, but with subtle differences that will be discussed later. We consider first the agreement between the band structure and the room-temperature data. The best fit between experiment and theory as shown in Fig. 3 is obtained with $E_0=13.0$ eV. A rigid shift of the initial state bands by 0.2 eV to higher binding energies is also required in order to match the data as a whole, especially the experimental feature at $\leqslant 0.9$ eV binding energy with the minority (spin-down) transitions at photon energies between 40–53 eV. This is in fact the only possible fit for the latter feature, if it is recalled that the spin polarization is negative from the Fermi level down to approximately 1.7 eV at 200 K.[15] Its dispersion shows a clear maximum in binding energy at around 46 eV photon energy and therefore it is identified as emission from the Γ point. Once the Γ point is identified, the other critical point L in the symmetry line is fixed by Eq. (1), both of which are indicated by the dash-dotted lines in Figs. 3 and 4.

In order to examine in more detail the observed dispersion of the lowest binding energy feature at photon energies between 40–53 eV, the corresponding EDC's obtained at 300 K are shown in Fig. 5 on an expanded scale. Two bands, derived from a peak and a shoulder, instead of only one as in Fig. 3, are now observed in the spectra. The band in Fig. 3 is therefore the intensity-weighted average of the two bands resulting from the smoothing applied to the EDC's in the second-derivative method. The two bands thus appear to correspond to the first two occupied minority-spin bands in the calculation, both of which disperse upward towards the zone boundary. The energies at the Γ point of the two bands estimated from Fig. 5 are listed in Table I and are compared with results from all the calculations. The calculation of ZS gives the best agreement with experiment in terms of the position and separation of these two features. Furthermore, YH predict two occupied majority-spin bands above the first minority-spin band around the Γ point, which was not the case in the earlier calculations.[11,12] Features that might be due to emission from these majority-spin bands near the Γ point are either not present or might be too weak to be seen in the spectra.

On cooling to 90 K, no appreciable changes are observed in this region of the spectra near the Fermi edge within the range of photon energies used (see Fig. 4). Chainani *et al.*[23] have, however, reported photoemission experiments on

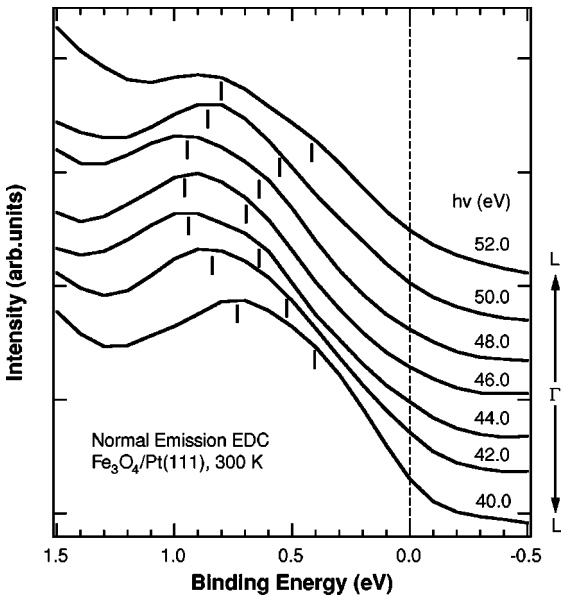

FIG. 5. A selection of normal emission spectra taken at 300 K showing the dispersion of the lowest binding energy features (indicated by the vertical bars). The turning point in the dispersion corresponds to the Γ point.

cleaved $Fe_3O_4(110)$ surfaces and found a downwards shift of about 70 meV of the Fermi edge when their sample was cooled from 300 to 100 K, consistent with the characteristics of the Verwey transition. The energy resolution in the present experiments was probably not sufficient to observe such a small change. Nevertheless, one would expect the opening up of a band gap at the point where the first minority-spin band in the high-temperature phase is expected to cross the Fermi level in order to explain the Verwey transition from the band structure point of view. Following the dispersion observed in Fig. 5, a crossing should occur at a photon energy <40 or >54 eV. Because of the lack of data at photon energies <40 eV and of the interference of resonant photoemission at photon energies >54 eV (see below), we are unable to confirm the above possibility in the present study.

For the rest of the data in Fig. 3, the weak transitions can be assigned equally well to either the majority-spin bands or the minority-spin bands, but the strong features agree better with the calculated transition lines for the minority-spin bands. This is particularly true for the strong feature around 4.0 eV for $h\nu<56$ eV and that around 5.5 eV for $h\nu>70$ eV. These two features appear to be parts of the same calculated band, which disperses downward from 3.5 eV at Γ to about 5.0 eV at the zone boundary L where a small gap opens. It then extends into the next zone and disperses to 5.5 eV at $h\nu=80$ eV. The gap is not visible in the experimental data, but the band folding at the zone boundary (circled in Fig. 3) can be seen. On the other hand, there is a majority-spin band with similar dispersion which might also be assigned to these strong transitions. The energies, however, differ substantially from those in the experiments. The present comparison therefore suggests that they are a minority-spin band. Since the thin film was not magnetized throughout its preparation, it is unlikely that this apparently better agreement is due to a preferential domain orientation. The problem may simply be due to some inaccuracy in the calculated band energies. This is possible since the fit shown in the structure plots has been obtained by shifting the entire calculated band structure by 0.2 eV towards higher binding energy. The critical point energies listed in Table I also show differences compared to the experimental values of up to 0.4 eV. These differences are sufficient to suggest an alternative assignment of these strong features. The actual situation may be that they contain contributions from both the majority- and minority-spin bands; a precise identification can only be achieved with spin- and angle-resolved photoemission experiments.

We now discuss the subtle differences between the data taken at 300 K and at 90 K, as well as some general effects caused by the resonant photoemission. The most interesting difference can be seen within the circled regions in Figs. 3 and 4. In the data taken at 300 K, as stated above, folded transitions from the zone boundary L are present, whereas at 90 K no such band folding is observed. The absence of folded transitions at the lower temperature is consistent with the change of the crystallographic symmetry associated with the Verwey transition:[25] the L point is no longer a Brillouin zone boundary of the monoclinic structure at low temperature. Temperature-dependent changes to the highest binding energy feature may also be due to the altered symmetry: at 300 K, this band shows a large energy dispersion with photon energy conforming roughly with the periodicity of the cubic phase; at 90 K it becomes much flatter.

As for the effects of resonant photoemission, we note that the dispersion of the features discussed above is strongly affected as the photon energy is scanned across the threshold energy (56 eV) for the Fe $3p\rightarrow3d$ excitation. There is a discontinuity in the behavior of the lowest binding energy feature at $h\nu=54$ eV, i.e., 2 eV below the threshold energy. This is related to its resonant behavior (see Sec. III B). For $h\nu>54$ eV, this feature appears to be associated more with the occupied majority-spin bands near E_F. Moreover, a strong feature around 3.5 eV binding energy appears just above the threshold energy (56 eV) and does not seem to correspond to any of the calculated transitions. Its dispersion shows also a slight temperature dependence. All these features with binding energies above 4 eV are mainly of Fe $3d$ origin according to band-structure calculations.[11,12,33] Finally, resonant photoemission appears not to produce any discontinuities in the dispersion of the weak transitions at

TABLE I. Critical energies at the Γ point of the first two occupied minority-spin bands.

Symmetry	YS (Ref. 11) (eV)	ZS (Ref. 12) (eV)	YH (Ref. 33) (eV)	Expt. (eV)
Γ_1	-0.26	-0.44	-0.52	-0.70 ± 0.08
Γ_{12}	-0.65	-0.65	-0.54	-0.95 ± 0.08

binding energies around 5.5 and 8 eV. The density of these states contains both contributions from Fe $3d$ and O $2p$ electrons, although the O $2p$ character increases with increasing binding energy.[11,12,33] The effect of resonant photoemission, which involves mainly Fe $3d$ electrons,[19,29] may therefore be weaker.

To summarize the effect of the Verwey transition on the valence-band photoemission spectra, we note that there appear to be two types of changes in the valence-band spectra: Weak features from the lower-lying O $2p$-dominated valence bands show differences that are likely to be related to the changes in the crystallographic symmetry, whereas the behavior seen for the strong features of the higher-lying Fe $3d$-derived bands does not appear to be correlated to the structural changes. Because of their $3d$ origin, the differences are possibly caused by the charge ordering at the B site below the transition temperature.

B. Resonant photoemission

We now discuss the resonant enhancement of photoemission observed in Fig. 2 at the Fe $3p \rightarrow 3d$ excitation threshold at 56 eV. The mechanism of resonant photoemission in $3d$ transition metals and their compounds is well known.[42] From the localized-electron point of view, it is caused by the final-state interference between direct photoemission from the $3d$ levels ($3d^n \rightarrow 3d^{n-1} + e$) and Auger electron emission ($3p^6 3d^n \rightarrow 3p^5 3d^{n+1} \rightarrow 3p^6 3d^{n-1} + e$) following the $3p \rightarrow 3d$ core excitation. For iron oxides and other late transition-metal oxides, it is generally believed that the $3p \rightarrow 3d$ excitations are quite localized and involve only $3d$-derived states. Therefore, an approach has been used[18,19,29] in which the difference between the valence-band EDC's measured just above (on) and below (off) the resonance is used to remove the nonresonant O $2p$ contributions. The resulting features reflect the $3d$-derived final states. By performing constant-initial-state (CIS) measurements these $3d$ states can be further identified as either d^{n-1} or $d^n L$ final states, because d^{n-1} final states usually show a typical Fano-type resonance line shape, whereas for $d^n L$ final states an antiresonance behavior is expected with a dip on the lower photon energy side of the Fano peak.[43,44]

On the other hand, it has been observed that the photon energies corresponding to on and off resonance depend slightly on the valency of the Fe ions in the oxides. For α-Fe_2O_3 with only Fe^{3+} ions, they are found to be at 58 and 55 eV for on and off resonance, respectively.[19,29] For FeO, which contains only Fe^{2+} ions, Fujimori *et al.*[29] reported values of 57 and 53 eV, whereas Lad and Henrich[19] found the off-resonance energy to be 54 eV. The disagreement is due to the observation of a shoulder at 54 eV in the CIS spectra taken by Fujimori *et al.* for FeO, which is not present in the data of Lad and Henrich. For Fe_3O_4, which contains both Fe^{2+} and Fe^{3+} ions, Lad and Henrich[19] measured spectra on and off resonance at 58 and 54 eV, respectively. For the epitaxial $Fe_3O_4(111)$ film investigated here the corresponding photon energies depend slightly on the binding energy of the resonating states and are found mostly at 58 and 53 eV (see below and Fig. 7). At 54 eV, a weak bump can be seen from our CIS spectra for binding energies of 3.5, 5.6, and 8.0 eV.

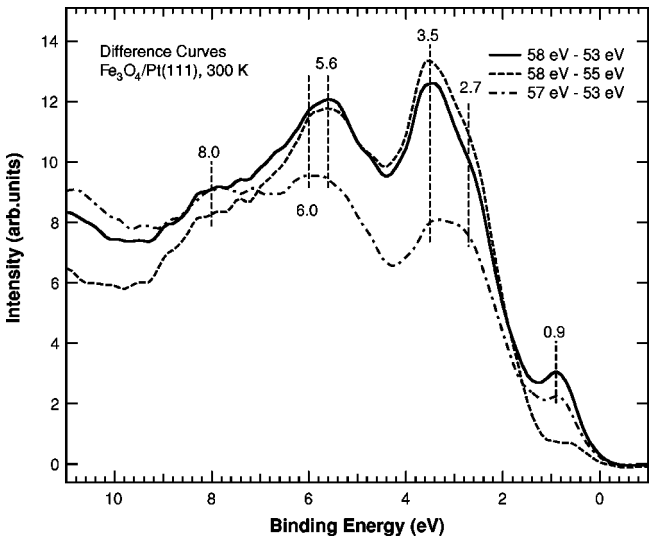

FIG. 6. Difference curves for normal emission spectra taken at 300 K just above and below the Fe $3p \rightarrow 3d$ resonant photoemission. Vertical dashed lines indicate the Fe $3d$-derived final states involved in the resonance.

It may therefore be possible, as suggested by Lad and Henrich,[19] to partially separate the contributions to the resonant photoemission in Fe_3O_4 from Fe^{2+} and Fe^{3+} ions by taking difference curves from EDC's taken at the on- and off-resonance photon energies of the corresponding iron valencies. Due to the proximity of these energies, however, one often finds overlapping contributions from both ions, and a separation may not always be possible or even meaningful, as will be seen in the following.

The difference curves from the normal emission data taken at 300 K are presented in Fig. 6 for $58-53$ eV, $58-55$ eV, and $57-53$ eV. Some distinct features can be identified readily and are marked by vertical dashed lines. They include a small peak at 0.9 eV, a shoulder at 2.7 eV, and peaks centered around 3.5, 5.6, and 8 eV. The broad satellite centered at 14 eV in Fig. 2, which also resonates strongly, is not shown in this figure. The CIS spectra for the corresponding binding energies (including that of the 14-eV satellite) are presented in Fig. 7. Based on their behavior in Figs. 6 and 7, some conclusions can be drawn as to the origin of these features. First, the 0.9-eV peak appears only in the difference curves for $58-53$ eV and $57-53$ eV, but apparently not in that for $58-55$ eV corresponding to the Fe^{3+}-related on- and off-resonance energies. It is therefore related only to final states of the Fe^{2+} ions. In fact, this feature has been assigned in earlier studies to a state of the $d^6 L$ final-state multiplet involving charge transfer between the cation $3d$ and the ligand $2p$ orbitals.[28,29] Experimentally it appears only when there are Fe^{2+} ions in the oxides (FeO and Fe_3O_4).[19,27–29] Its resonant behavior shows a Fano line shape with an antiresonance dip (see Fig. 7) at 53 eV and a maximum around 55 eV, which is also in agreement with the assignment to a $d^6 L$ final state.

For the other features observed, the situation is not as simple. Compared to the peak at 3.5 eV, for example, the shoulder at 2.7 eV becomes more prominent in the $57-53$ eV difference curve than in the others. This would suggest that it is dominated by final states of the Fe^{2+} ions. Its

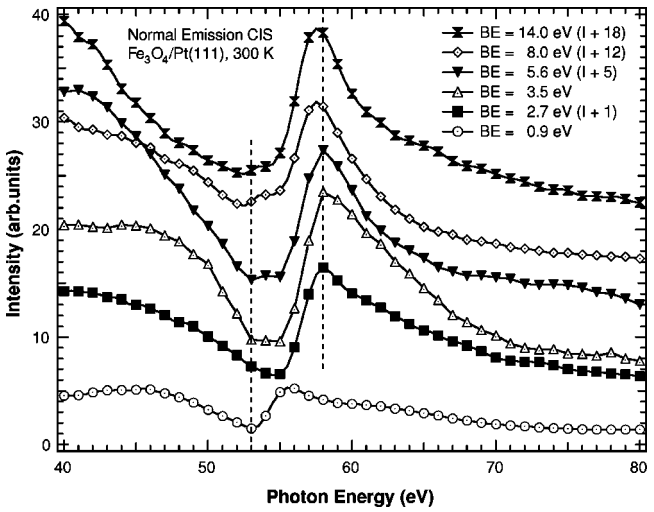

FIG. 7. Normal emission constant-initial-state spectra taken at 300 K for initial-state energies shown in Fig. 6. Vertical dashed lines mark the on- and off-resonance position. The background contributions have not been removed. For clarity, some spectra are shifted up by the amount indicated in brackets in the legend.

resonance behavior as shown in Fig. 7, however, has an on-resonance photon energy of 58 eV and an off-resonance photon energy of 55 eV, typical for final states originating from Fe^{3+} ions. The same analysis can be applied to the features seen at 3.5 and 5.6 eV and leads to similar conflicting conclusions. The small shoulder seen at 6.0 eV, not mentioned so far, is an exception. It has a resonance profile almost identical to that of the 5.6-eV feature (not shown for this reason). The above analysis would indicate that it is a final state of the Fe^{2+} ions. We therefore conclude that in most cases the characteristics of resonant photoemission observed in FeO and α-Fe_2O_3 cannot be used straightforwardly to separate contributions from the Fe^{2+} and Fe^{3+} ions in Fe_3O_4.

Nevertheless, the resonance profiles in Fig. 7 show that apart from the broad satellite centered at 14 eV, all the other features show a Fano-type resonance line shape with an antiresonance dip to a certain degree, whereby the dip for the feature at 3.5 eV is the strongest. This indicates that all these features are final states with a ligand hole $\underline{L}$. On the other hand, the satellite feature at 14 eV does not have an antiresonance dip in its resonance profile and is therefore a final state of d^{n-1} type. Given the above discussion, however, it is unclear whether this is associated with the Fe^{2+} or the Fe^{3+} ions, although the on-resonance photon energy is moved towards 57 eV supporting the assignment to Fe^{2+}.

Our assignments of the above $3d$-derived final states are in essential agreement with previous resonant photoemission studies of $Fe_3O_4(110)$ by Lad and Henrich.[19] The binding energies of the resonating states were found, however, at around 1.2, 4, 7, and 12 eV, somewhat different from the values obtained in Fig. 6 for the present $Fe_3O_4(111)$ film. Our difference curves shown in Fig. 6 also reveal more features than previously observed.[19] These differences may be understood on the basis of crystal anisotropy and band structure effects. This is because the resonant photoemission involves direct photoemission from the $3d$ levels, which is determined by the initial- and final-state band structures, and despite the Coulomb interaction in the Auger decay the wave vector remains a good quantum number. Valence-band dispersion of a sharp resonance in photoemission from LaSb has been reported and is interpreted in the same way.[45] In our case, the on- and off-resonant photon energies differ substantially, as do the corresponding wave vectors perpendicular to the surface. A variation in the matrix element may also be responsible for some of the features observed in the difference curves.

The main features observed in Fig. 6 are also observed in the data taken at 90 K. The spectral shapes are very similar, with the main peaks around 3.5 and 5.6 eV being somewhat broader and the centers of gravity moving towards lower binding energies. These changes are likely to be caused by changes in the initial states associated with the Verwey transition, as discussed in Sec. III A. The corresponding resonance profiles reveal virtually the same behavior for the same feature observed in the difference curves, indicating that the Verwey transition does not change the nature of the final states involved in the resonant photoemission. This demonstrates that resonant photoemission is indeed a localized process on which neither a charge ordering at the cation B site nor crystallographic symmetry variations would have any noticeable effect.

IV. SUMMARY

In summary, the valence-band structure of $Fe_3O_4(111)$ along the ΓL symmetry line and the resonant enhancement of photoemission across the Fe $3p \rightarrow 3d$ excitation threshold have been examined in detail both at 90 and 300 K. The experimentally derived band dispersions agree reasonably well with band-structure calculations for the high-temperature phase. In particular, dispersions of the minority-spin bands near the Fermi level predicted by the calculations are clearly observed. Together with the observation of finite intensity at the Fermi level this confirms the metallic nature of Fe_3O_4 magnetite. At 90 K, which is below the Verwey transition temperature, there are subtle differences in the valence-band spectra that may be attributed to the change in crystallographic symmetry and/or the charge ordering at the B site associated with the transition. Changes that may be related to the altered crystallographic symmetry are more pronounced in the lower-lying O $2p$-dominated bands, whereas changes observed for the strong features in the higher-lying Fe $3d$-derived bands are more likely caused by the charge ordering at the B site.

Resonant photoemission behavior is not changed at temperatures above and below the Verwey transition temperature, demonstrating the local character of this process that is not influenced by either a crystallographic symmetry change or a long-range order of the cations at the B site. This local character is also indicated by the observation of band discontinuities at the Fe $3p \rightarrow 3d$ resonance photon energy for the high-lying Fe $3d$-derived bands, whereas the low-lying O $2p$-dominated bands are not affected. The present results further indicate that, except for the resonant feature at 0.9 eV binding energy, most of the other resonant features in Fe_3O_4

cannot be separated into contributions from the Fe^{2+} or Fe^{3+} ions by comparing measured on- and off-resonance energies with those in FeO and Fe_2O_3, because Fe_3O_4 has its own characteristic band-structure and is not a simple superposition of FeO and Fe_2O_3. Furthermore, it is found that crystal anisotropy and band-structure effects may influence the energies of the resonant features observed in the difference curves, in further support of the itinerant-electron point of view for the interpretation of the electronic structure of magnetite.

ACKNOWLEDGMENTS

The authors gratefully acknowledge stimulating discussions with Professor A. Yanase and Professor N. Hamada and their permission to use unpublished data. We would also like to thank M. Swoboda and the BESSY staff for technical support. This work has been supported by the German Federal Ministry of Education, Science, Research and Technology (BMBF) under Contract No. 05 625EBA 6. One of us (Y.Q.C.) thanks the Max-Planck-Gesellschaft for financial support.

*Author to whom correspondence should be addressed. Present address: Institute for Solid State Physics, University of Tokyo, 7-22-1 Roppongi, Minato-ku, Tokyo 106-8666, Japan. Electronic address: cai@surface.issp.u-tokyo.ac.jp

[1] W. Weiss and G. A. Somorjai, J. Vac. Sci. Technol. A **11**, 2138 (1993); W. Weiss, A. Barbieri, M. A. Van Hove, and G. A. Somorjai, Phys. Rev. Lett. **71**, 1848 (1993), and references therein.

[2] A. Barbieri, W. Weiss, M. A. Van Hove, and G. A. Somorjai, Surf. Sci. **302**, 259 (1994).

[3] Th. Schedel-Niedrig, W. Weiss, and R. Schlögl, Phys. Rev. B **52**, 17 449 (1995).

[4] D. M. Lind, S. D. Berry, G. Chern, H. Mathias, and L. R. Testardi, Phys. Rev. B **45**, 1838 (1992), and references therein.

[5] P. J. Chen and D. W. Goodman, Surf. Sci. **312**, L767 (1994).

[6] N. Tsuda, K. Nasu, A. Yanase, and K. Siratori, *Electronic Conduction in Oxides* (Springer-Verlag, Berlin, 1991).

[7] W. Weiss, M. Ritter, D. Zscherpel, M. Swoboda, and R. Schlögl, J. Vac. Sci. Technol. A **16**, 21 (1998).

[8] N. F. Mott, Philos. Mag. B **42**, 327 (1980), and the other articles in the same series.

[9] D. L. Camphausen, J. M. D. Coey, and B. K. Chakraverty, Phys. Rev. Lett. **29**, 657 (1972).

[10] D. Ihle and B. Lorenz, Philos. Mag. B **42**, 337 (1980).

[11] A. Yanase and K. Siratori, J. Phys. Soc. Jpn. **53**, 312 (1984).

[12] Z. Zhang and S. Satpathy, Phys. Rev. B **44**, 13 319 (1991).

[13] S. K. Mishra, Z. Zhang, and S. Satpathy, J. Appl. Phys. **76**, 6700 (1994).

[14] S. G. Bishop and P. C. Kemeny, Solid State Commun. **15**, 1877 (1974).

[15] S. F. Alvarado, W. Eib, F. Meier, D. T. Pierce, K. Sattler, and H. C. Siegmann, Phys. Rev. Lett. **34**, 319 (1975); S. F. Alvarado, M. Erbudak, and P. Munz, Phys. Rev. B **14**, 2740 (1976).

[16] C. R. Brundel, T. J. Chuang, and K. Wandelt, Surf. Sci. **68**, 459 (1977).

[17] S. Vasudevan, M. S. Hegde, and C. N. R. Rao, J. Solid State Chem. **29**, 253 (1979).

[18] K. Siratori, S. Suga, M. Taniguchi, K. Soda, S. Kimura, and A. Yanase, J. Phys. Soc. Jpn. **55**, 690 (1986).

[19] R. J. Lad and V. E. Henrich, Phys. Rev. B **39**, 13 478 (1989); J. Vac. Sci. Technol. A **7**, 1893 (1989).

[20] F. M. F. de Groot, M. Grioni, J. C. Fuggle, J. Ghijsen, G. A. Sawatzky, and H. Petersen, Phys. Rev. B **40**, 5715 (1989).

[21] M. Sancrotti, F. Ciccacci, M. Finazzi, E. Vescovo, and S. F. Alvarado, Z. Phys. B **84**, 243 (1991).

[22] Y. Ma, P. D. Johnson, N. Wassdahl, J. Guo, P. Skytt, J. Nordgren, S. D. Kevan, J.-E. Rubensson, T. Böske, and W. Eberhardt, Phys. Rev. B **48**, 2109 (1993).

[23] A. Chainani, T. Yokoya, T. Morimoto, T. Takahashi, and S. Todo, Phys. Rev. B **51**, 17 976 (1995).

[24] E. J. W. Verwey and P. W. Haaymann, Physica (Amsterdam) **8**, 979 (1941); E. J. W. Verwey, P. W. Haayman, and F. C. Romeijn, J. Chem. Phys. **15**, 181 (1947).

[25] J. Yoshida and S. Iida, J. Phys. Soc. Jpn. **42**, 230 (1977); S. Iida, Philos. Mag. B **42**, 349 (1980).

[26] S. Sugano, Y. Tanabe, and H. Kamimura, *Multiplets of Transition-Metal Ions in Crystals* (Academic, New York, 1970).

[27] D. E. Eastman and J. L. Freeouf, Phys. Rev. Lett. **34**, 395 (1975).

[28] P. S. Bagus, C. R. Brundle, T. J. Chuang, and K. Wandelt, Phys. Rev. Lett. **39**, 1229 (1977).

[29] A. Fujimori, M. Saeki, N. Kimizuka, M. Taniguchi, and S. Suga, Phys. Rev. B **34**, 7318 (1986); A. Fujimori, N. Kimizuka, M. Taniguchi, and S. Suga, *ibid.* **36**, 6691 (1987).

[30] J. Zaanen, G. A. Sawatzky, and J. W. Allen, Phys. Rev. Lett. **55**, 418 (1985).

[31] F. Ciccacci, L. Braicovich, E. Puppin, and E. Vescovo, Phys. Rev. B **44**, 10 444 (1991).

[32] L. Braicovich, F. Ciccacci, E. Puppin, A. Svane, and O. Gunnarsson, Phys. Rev. B **46**, 12 165 (1992).

[33] A. Yanase and N. Hamada (unpublished); A. Yanase, ISSP Diaries **37**, 66 (1997) (in Japanese).

[34] M. Ritter, W. Ranke, and W. Weiss, Phys. Rev. B **57**, 7240 (1998).

[35] The weak and broad feature close to the binding energies of the Pt $4f$ core lines in spectrum (b) of Fig. 1 is due to emission from the $M_{2,3}M_{4,5}M_{4,5}$ super-Coster-Kronig Auger transitions in the oxide (Ref. 29).

[36] M. Krumrey, E. Tegeler, J. Barth, M. Krisch, F. Schäfers, and R. Wolf, Appl. Opt. **27**, 4336 (1988).

[37] V. C. Rakhecha and N. S. Satya Murthy, J. Phys. C **11**, 4389 (1978).

[38] It should, however, be pointed out that the local-density approximation (LDA) within the density-functional formalism is known to underestimate the optical band gap for many systems including transition metal oxides [see, e.g., O. K. Andersen, H. L. Skriver, and H. Nohl, Pure Appl. Chem. **52**, 93 (1979)]. It is generally recognized that one would need to go beyond the LDA in order to obtain a correct band gap and correct conduction-band energies [see, e.g., A. Svane and O. Gunnarsson, Phys. Rev. Lett. **65**, 1148 (1990)].

[39] Strictly speaking, the data taken at 90 K should be compared with band-structure calculations for magnetite in the low-temperature phase. However, to the best of our knowledge, such calculations are still lacking in the literature. The comparison here is therefore only for the purpose of identifying the differences and similarities between the data taken at 90 and 300 K.

[40] This procedure is not without pitfalls. Care has therefore been taken to ensure that the resulted peaks and shoulders match the smoothed experimental spectra.
[41] See, e.g., S. Hüfner, *Photoelectron Spectroscopy: Principles and Applications* (Springer-Verlag, Berlin, 1995).
[42] For a review, see, L. C. Davis, J. Appl. Phys. **59**, R25 (1986).
[43] L. C. Davis, Phys. Rev. B **25**, 2912 (1982).
[44] A. Fujimori and F. Minami, Phys. Rev. B **30**, 957 (1984).
[45] C. G. Olson, P. J. Benning, M. Schmidt, D. W. Lynch, P. Canfield, and D. M. Wieliczka, Phys. Rev. Lett. **76**, 4265 (1996).